Supporting information

Graphene nanoribbons from unzipped carbon nanotubes: atomic structures, Raman spectroscopy and electrical properties

Liming Xie,[1,†] Hailiang Wang,[1,†] Chuanhong Jin,[2] Xinran Wang,[1]
Liying Jiao,[1] Kazu Suenaga,[2] Hongjie Dai[1,*]

[1]*Department of Chemistry, Stanford University, California 94305, USA*

[2]*Nanotube Research Center, National Institute of Advanced Industrial Science and Technology (AIST), Tsukuba 305-8565, Japan*

[†]These authors contributed equally to this work.

[*]To whom correspondence should be addressed: hdai1@stanford.edu

Part 1. Materials and Methods

Sample Preparation

GNRs were produced by unzipping arc-discharge grown multi-walled carbon nanotubes (MWNTs)[1]. MWNTs (30 mg; Aldrich, 406074-500MG) were calcined at 500 ^{o}C in a furnace for 1 h. The calcined nanotubes (15 mg) and 7.5 mg PmPV (Aldrich, 555169-1G) were then dissolved in 10 ml 1,2-dichloroethane and sonicated (Cole Parmer sonicator, model 08849-00) for 1 h. The solution was ultracentrifuged (Beckman L8-60M ultracentrifuge) at 40,000 rpm for 2 h. For TEM sample preparation, silicon membrane window grids (SPI Supplies, US200-P15Q UltraSM 15 nm Porous TEM Windows) were soaked in the GNR solution overnight. The grid with GNRs deposited was calcined in air at 350 ^{o}C for 30 min to remove polymer coating on the GNRs to a small extent.

GNRs on SiO_2/Si substrates (SiO_2 thickness of 300 nm) were prepared by spin-coating a GNR suspension on SiO_2/Si substrates followed by calcination in air at 350 ^{o}C for cleaning. The samples were used for AFM, micro-Raman measurements and/or electrical device fabrication. For GNRs characterized by Raman spectroscopy

and followed by device fabrication, relatively long GNRs (~2 μm) with the lowest topographic heights (in the range of 1.0-1.2 nm) were selected. Raman mapping was done near one end of the ribbon and devices were fabricated on the other end of the ribbon without laser irradiation.

TEM Characterizations

Low-resolution TEM was done on an FEI Tecnai G2 F20 X-TWIN TEM instrument at an operation voltage of 200 kV at Stanford University. High-resolution, aberration-corrected TEM was done at an operation voltage of 80 kV on TEAM 0.5 [2] at the Lawrence Berkeley National Laboratory and at an operation voltage of 60 kV on a JEOL 2100F TEM with the DELTA correctors[3] (including an imaging aberration corrector) at the Nanotube Research Center, National Institute of Advanced Industrial Science and Technology (AIST) in Japan.

AFM Characterizations

AFM was done on a Vecco IIIa nanoscope using the tapping mode. Tip convolution was calibrated in the width measurements of GNRs using the same method in the reference[4]. AFM was used to locate GNRs relative to pre-fabricated alignment markers and the registered ribbons were used for subsequent micro-Raman and device fabrication experiments. In detail, large scale AFM image, such as 12 μm by 12 μm, was taken with maker and GNRs included in the image (Figure S1a). The position of the individual GNRs were measured relatively to the maker. After that, the sample was put under Raman microscope, the marker was directly seen under optical microscope and then the locations of individual GNRs were derived. Raman mapping was used to further confirm the GNRs and also to image the GNR axis directions (Figure S1c).

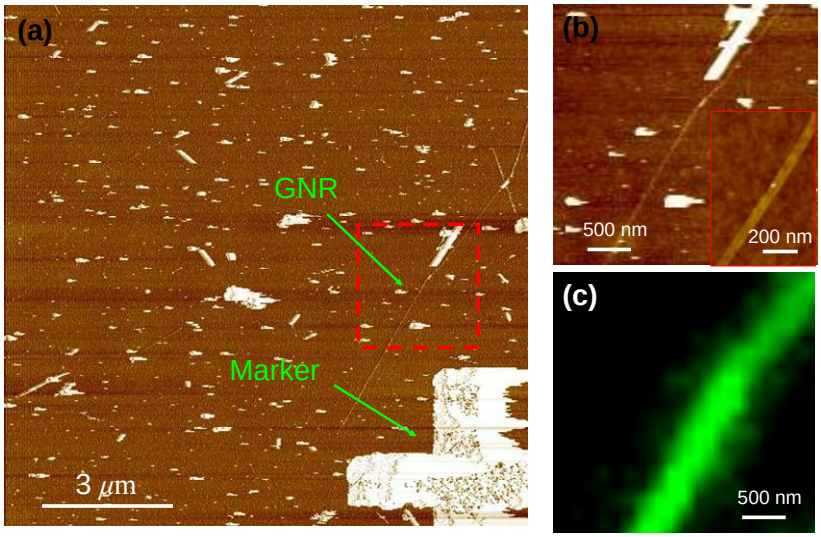

Figure S1 (a) Large scale AFM image (phase image) of GNRs on SiO_2/Si substrate. Relative position of the GNRs to the maker can be determined from the AFM image. (b) Zoomed-in AFM images and (c) Raman mapping (D band intensity) of the area indicated by the red dash box in panel a. The inset in (b) shows a high resolution AFM image of the GNR.

Polarized Raman Measurements

Polarized Raman measurements were done on a Horiba HR800 Raman system with 532 nm excitation. The laser power was kept at ~1 mW/μm^2 during Raman measurements. A 100x objective and a 300 lines/mm grating was used, corresponding to a spatial resolution of ~0.5 μm and a spectrum resolution of ~2 cm^{-1}. A half-wave plate was put in the laser path to rotate the polarization of the laser (Fig. S2a). An analyzer was put in the signal path to select the polarization of the Raman signal (Fig. S2a). The GNR direction (with an accuracy of +/- 5^o) was measured by both AFM imaging and Raman mapping.

Polarized Raman measurements were done in the *VV* configuration (Fig. S2b), in which the polarization directions of the laser and the Raman signal were kept parallel and the Raman spectra were collected at different angles between the laser-Raman polarization direction and the GNR direction. Typical Raman accumulation time was 14 s. Polarization dependent response of the Raman system was calibrated by using Raman bands of graphite. In detail, an analyzer was put in the signal path to yield polarized Raman signal and a half-wave plate was put after the analyzer. Polarization

dependent response of the Raman system was recorded while rotating the half-wave plate. The intensities of D band, G band, D' band and 2D (or G') band were extracted through Lorentzian peak fitting of the Raman spectra.

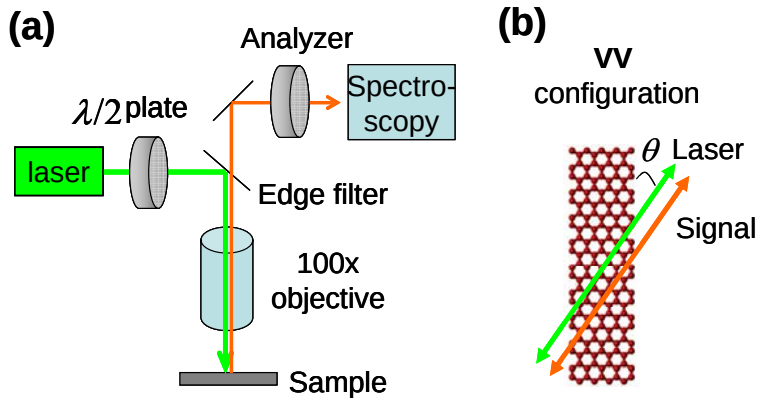

Figure S2 (a) Scheme of polarized Raman measurements. (b) Illustration of *VV* configuration. The green and orange arrows show the polarization directions of the laser and the analyzer, respectively. θ is the angle between the laser-Raman polarization direction and the GNR axis direction.

Electrical Devices and Measurements

Electrical devices were made for the same GNRs (at locations determined by AFM imaging) used in micro-Raman mapping experiments by electron-beam lithography followed by electron-beam evaporation of Pd (30 nm). The devices were annealed in Ar at 220 ^{o}C for 15 min to improve the contacts. Electrical measurements were done at room temperature in a home-built vacuum probe station and after electrical annealing[5] to clean the ribbons and observe the Dirac point of the GNR devices. The heavily doped Si substrate was used as a gate. The resistivity of an individual GNR, R, was calculated by $R = \left(\frac{V_{ds}}{I_{ds}}\right)_{V_{gs,Dirac\ point}} \frac{W}{L}$, where V_{ds} is the drain-source voltage, I_{ds} is the drain-source current, $V_{gs,\ Dirac\ point}$ is V_{gs} at the minimum conductance point, W is the width of the GNR in nm and L is the channel length of the GNR device in nm.

Part 2. Electron-beam (e-beam) layer-by-layer evaporation of GNRs.

The high energy electrons used in the TEM imaging can evaporate carbon atoms layer by layer[6], which can be used to count the layer numbers of GNRs.

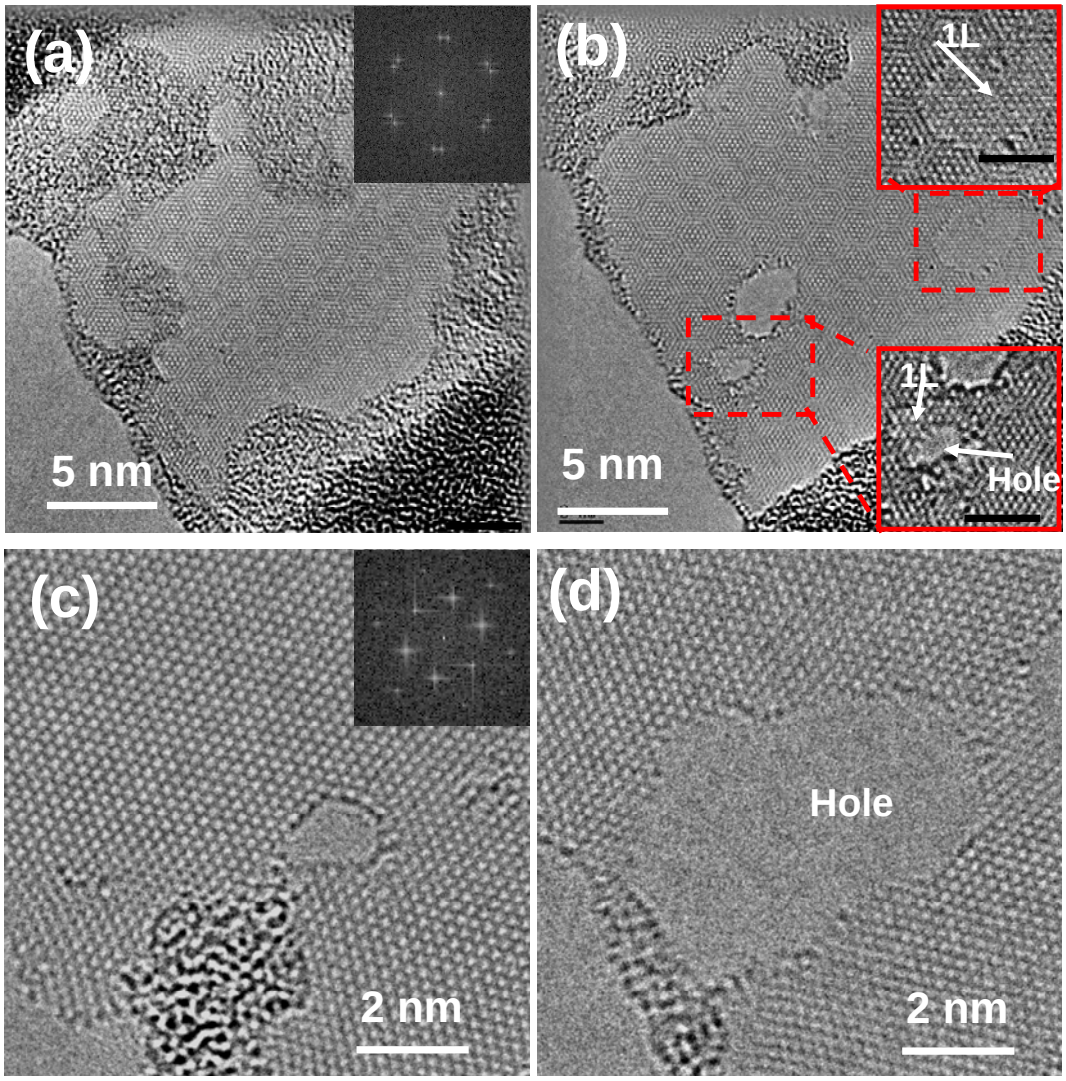

Figure S3 A GNR with two sets of hexagonal spots in the FFT image (a) before and (b) after a few minutes of e-beam irradiation. Coatings on the ribbons are polymer residues from GNR making process. The scale bars in panel (b) insets are 2 nm. A GNR with one set of hexagonal spots in the FFT image (c) before and (d) after e-beam irradiation. The insets in panels (a) and (c) are FFT images of the corresponding GNR regions in panels (a) and (c). Note: the simple FFT analysis is not always reliable to determine the layer number, because one could underestimate it if there is any well-ordered AA or AB stacking involved. Therefore it is essential to confirm the layer number by layer-by-layer ablation using a focused e-beam.

Part 3. TEM images of a GNR with straight edge lines at different tilting angles.

Figure S4 shows a GNR with straight edge lines at tilting angles of 0^{o} and 23^{o} with widths of 20.7 and 19.3 nm, respectively. This result is consistent with a model of tilting a flat ribbon. In detail, for a flat ribbon with a width of 20.7 nm and an angle of 14^{o} from the tilting angle, the projected width at a tilting angle of 23^{o} should be

$$\sqrt{[20.7 \bullet \sin(14^o)]^2 + [20.7 \bullet \cos(14^o) \bullet \cos(23^o)]^2}\ nm\ =\ 19.2\ nm$$

The observed width (19.3 nm) is 0.1 nm from the calculation, which is within the imaging resolution (~0.1 nm).

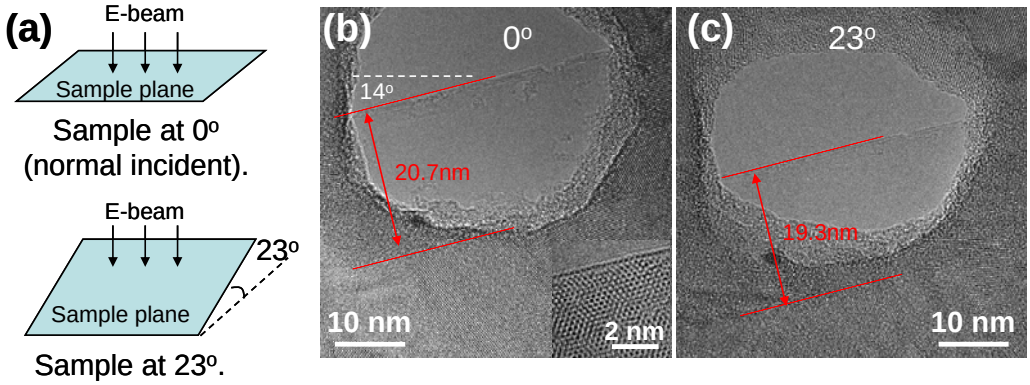

Figure S4 (a) Schematic illustration of imaging GNR sample at different titling angles. TEM of a GNR with straight edge lines at tilting angles of (b) 0^o and (c) 23^o. The GNR is 14^o from the tilting axis [the white dash line in panel (b)]. Inset in (b) shows a high resolution image of this GNR at tilting angle of 0^o.

Part 4. Layer-layer stacking in two-layer GNRs and chiral angles for all GNRs.

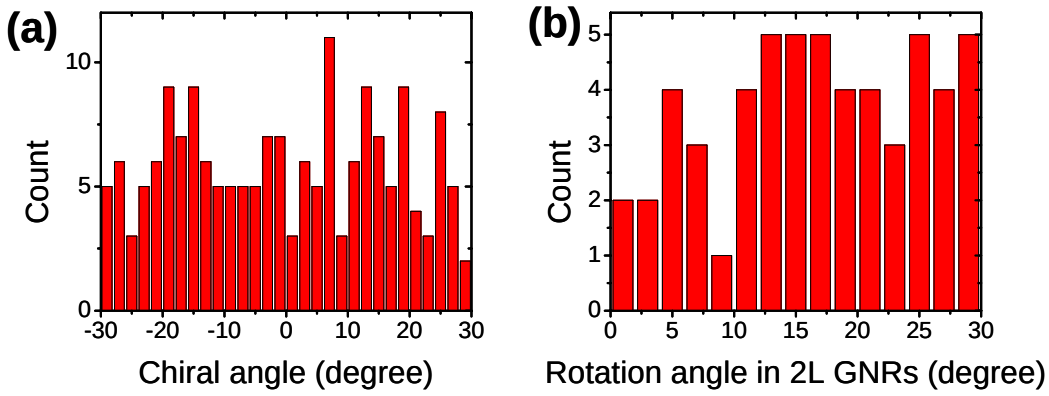

Figure S5 (a) Distribution of chiral angles for all imaged GNRs. (b) Distribution of layer-layer stacking in 2L GNRs.

Part 5. TEM images of a two-layer GNR with chiral angles of $0^o/8^o$.

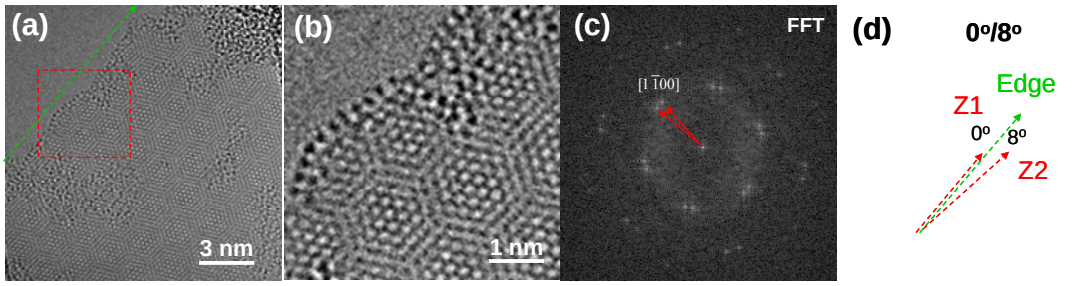

Figure S6 (a) Large-scale and (b) zoom-in TEM images of a 2L GNR with chiral angles of $0^{o}/8^{o}$. (c) FFT image of this two-layer GNR. The green dash arrows indicate the edge direction. The red arrows indicate the $[1\,\bar{1}00]$ directions for the two layers. (d) Chiral angle analysis. The zigzag directions (Z1 and Z2, indicated by red dash arrows) for the two layers are derived from the $[1\,\bar{1}00]$ directions in panel (c).

Part 6. AFM images and polarization dependence of D' and 2D band intensities for the GNRs in Figs. 3a-3d.

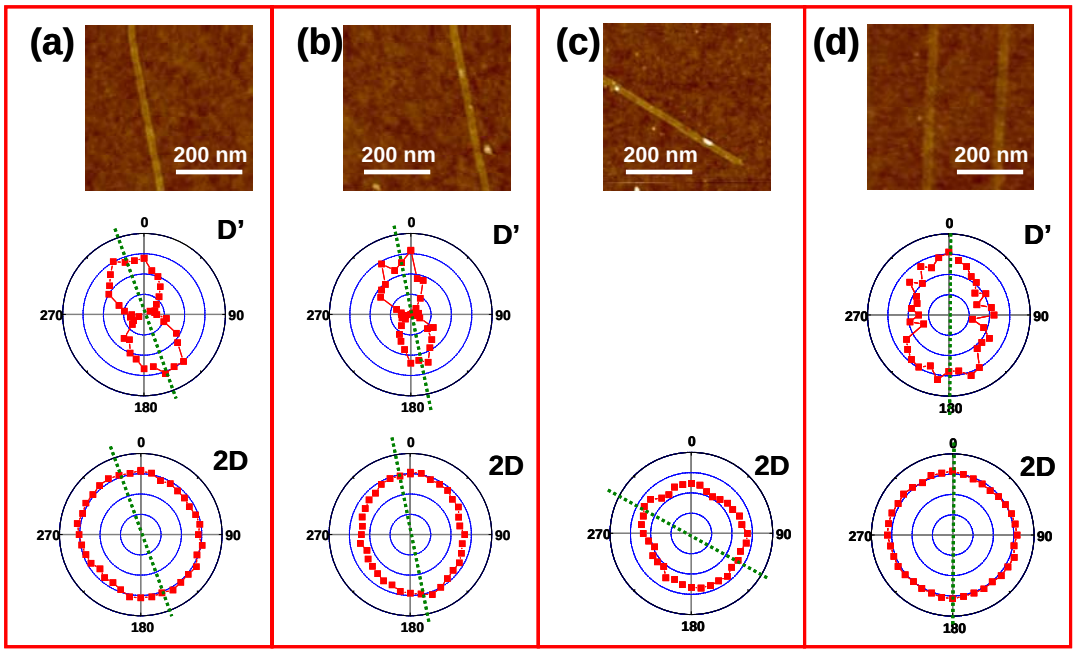

Figure S7 AFM images and polarization dependence of D' and 2D band intensities for the GNRs in (a) Fig. 3a, (b) Fig. 3b, (c) Fig. 3c and (d) Fig. 3d. The intensity scales in all polar plots are linear from zero. The green dash lines indicate the GNR directions. The D' band intensity for the GNR in panel (c) was too weak to be extracted out. The intensity scales in all polar plots are linear from zero. The green dash lines indicate the GNR directions.

Part 7. Polarized Raman measurements on individual few-walled CNTs.

Few-walled CNTs (mainly double-walled CNTs) were synthesized by chemical

vapor deposition[7] and was a gift from Dr. Jie Liu at Duke University.

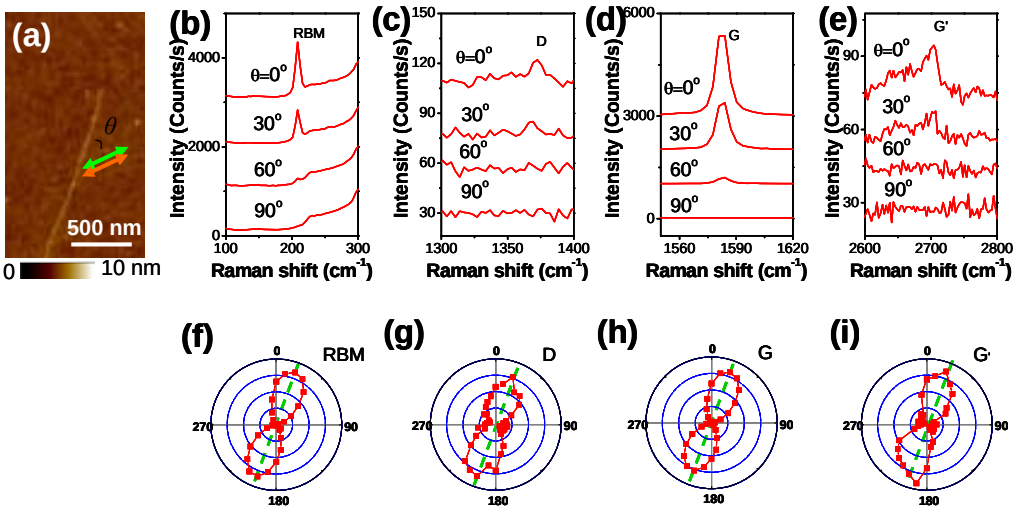

Figure S8 (a) AFM image of a few-walled CNT. Polarized Raman spectra of this CNT at different laser-Raman polarization to nanotube axis angles: (b) RBM band, (c) D band, (d) G band, and (e) G' band. Polarization dependent Raman intensity for (f) RBM band, (g) D band, (h) G band, and (i) G' band. The intensity scales in all polar plots are linear from zero. The green dash lines indicate the GNR direction.

Part 8. Polarized Raman measurements on individual MWNTs (the parent material used in unzipping experiments for obtaining GNRs used in this work).

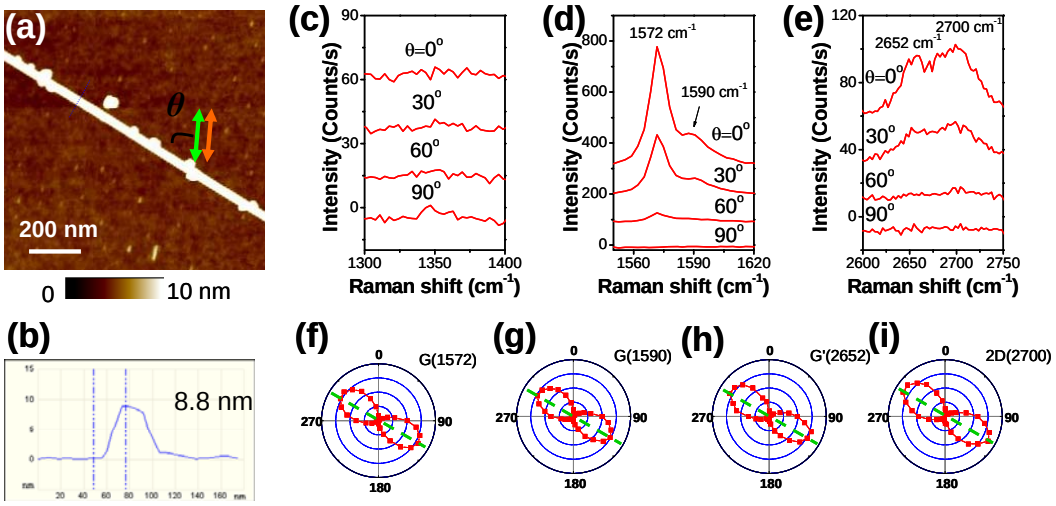

Figure S9 (a) AFM image of a MWNT. (b) Section analysis of this MWNT along the blue dash line in panel (a), showing a height of 8.8 nm. Polarized Raman spectra of this carbon nanotube at different laser-Raman polarization to nanotube axis angles: (c) 1300-1400 cm^{-1} range, (d) G band, and (e) G' band. Polarization dependent Raman intensity for (f) G band at 1572 cm^{-1}, (g) G band at 1590 cm^{-1}, (h) G' band at 2652 cm^{-1}, and (i) G' band at 2700 cm^{-1}. The intensity scales in all polar plots are linear from zero. The green dash lines indicate the GNR direction.

Part 9. Polarized Raman spectra of a GNR with an intermediate $D_{//}/G_{//}$ ratio of 2.7.

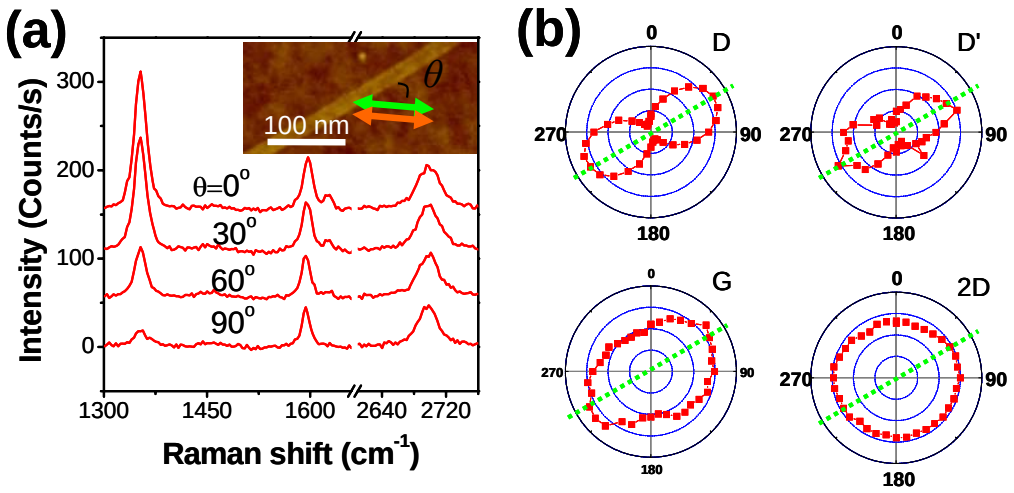

Figure S10 (a) Polarized Raman spectra of a GNR with an intermediate $D_{//}/G_{//}$ ratio of 2.7. The inset shows an AFM image of the GNR. (b) Plots of D, D', G and 2D band intensities to the angle between the laser-Raman polarization direction and the GNR direction. The intensity scales in all polar plots are linear from zero. The green dash lines indicate the GNR direction.

Part 10. Dependence of $D_{//}/G_{//}$ ratio and $D_{//}/D_{\perp}$ ratio on GNR width.

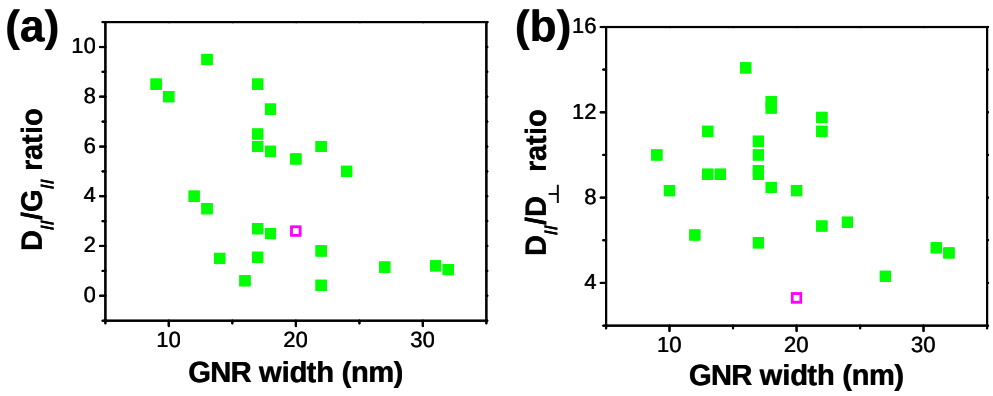

Figure S11 Dependence of (a) $D_{//}/G_{//}$ ratio and (b) $D_{//}/D_{\perp}$ ratio on GNR width. The hollow square is the data for Litho-GNRs in Fig. 3d.

Part 11. $2D_{//}/G_{//}$ ratio and 2D width vs. $D_{//}/G_{//}$ ratio for GNRs from unzipped MWNTs.

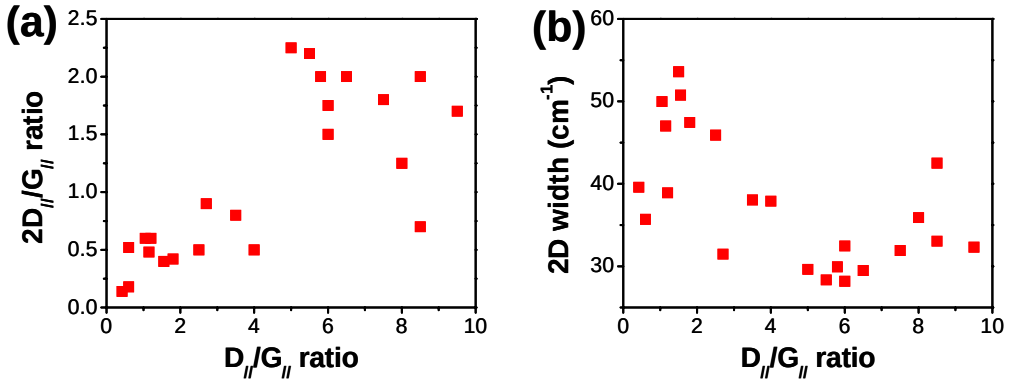

Figure S12 (a) $2D_{//}/G_{//}$ ratio and (b) 2D width vs. $D_{//}/G_{//}$ ratio for GNRs from unzipped MWNTs.

Part 12. Room-temperature electrical transport measurements of individual GNRs used in polarized Raman measurements.

Two GNRs with very different $D_{//}/G_{//}$ ratio of 6.5 and 0.6 (Fig. S13a and S13b with similar $D_{//}/D_{\perp}$) exhibited similar resistivity (see red and blue squares in Fig. S13e). This was consistent with that the $D_{//}/G_{//}$ ratio reflected average lattice orientation rather than defects in the GNRs. On the other hand, for two GNRs (Fig. S13b and S13d) with similar average chiral angles near 0^{o} ($D_{//}/G_{//}$ ratio ~ 0.6 and 0.4 respectively), the GNR with a higher $D_{//}/D_{\perp}$ ratio of 14 (Fig. S13b and the blue square

in Fig. S13e) exhibited lower resistivity than the GNR with a lower $D_{//}/D_{\perp}$ ratio of 6.7 (Fig. S13d and the cyan square in Fig. S13e). Similarly, for two GNRs with chiral angles closer to 30° (Figs. S13a and S13c, $D_{//}/G_{//}$ ratios of 6.5 and 7.5, respectively), the GNR with a higher $D_{//}/D_{\perp}$ ratio also exhibited a lower resistivity. For various GNRs measured, a discernable trend of lower resistivity for GNRs with higher $D_{//}/D_{\perp}$ ratios existed (Fig. S13f), consistent with reduced edge scattering in GNRs with smoother edges (higher $D_{//}/D_{\perp}$).

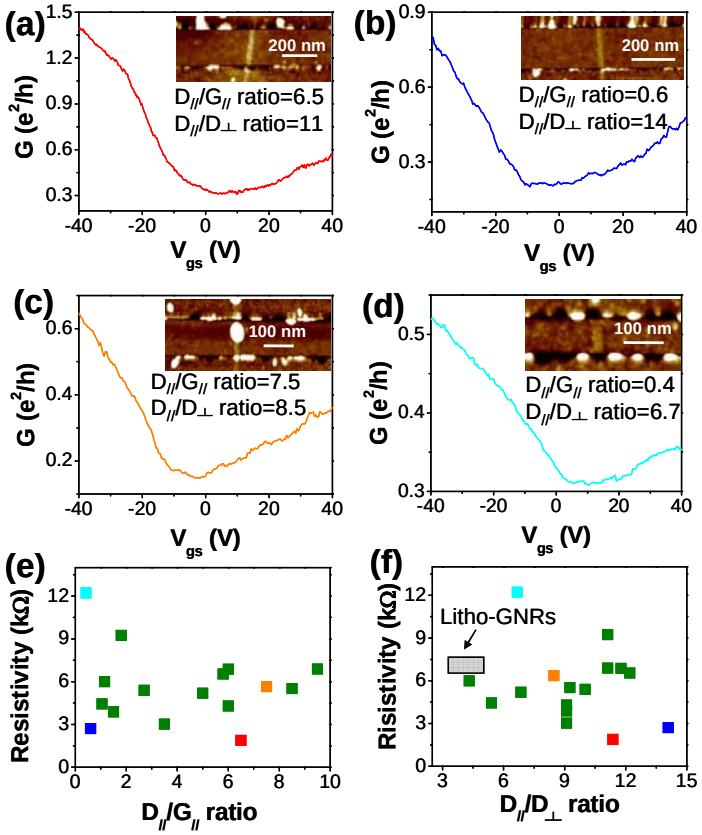

Figure S13. Room-temperature electrical transport measurements of GNRs used in polarized Raman measurements. (a)-(d) Conductance vs. gate voltage (V_{gs}) for four GNRs with $D_{//}/G_{//}$ and $D_{//}/D_{\perp}$ ratios indicated. The source-drain bias voltage (V_{ds}) was 10 mV. The insets are the AFM images of the corresponding GNR devices. (e) Plot of GNR resistivity vs. Raman $D_{//}/G_{//}$ ratio for various GNRs measured. (f) Plot of GNR resistivity vs. $D_{//}/D_{\perp}$ ratio for various GNRs. The red, blue, orange and cyan points in panels (e) and (f) are data points for the GNRs in panels (a)-(d) with curves in the corresponding colors. Note that we used AFM imaging to select a relatively small percentage of GNRs with apparent topographic heights in the lowest range of 1.0-1.2 nm (including polymer residues on the ribbon) for Raman and transport measurements. These ribbons were likely 1L GNRs with an average resistivity higher than that of 1-3 nm tall GNRs (a high percentage of two-layer ribbons) measured previously (ref. 1). Raman mapping for locating GNRs before polarized Raman measurements might also decrease the conductance of the GNRs measured in this paper.

References

(1) Jiao, L. Y.; Wang, X. R.; Diankov, G.; Wang, H. L.; Dai, H. J., *Nat. Nanotechnol.* **2010,** *5*, (5), 321-325.

(2) Kisielowski, C.; Freitag, B.; Bischoff, M.; van Lin, H.; Lazar, S.; Knippels, G.; Tiemeijer, P.; van der Stam, M.; von Harrach, S.; Stekelenburg, M.; Haider, M.; Uhlemann, S.; Muller, H.; Hartel, P.; Kabius, B.; Miller, D.; Petrov, I.; Olson, E. A.; Donchev, T.; Kenik, E. A.; Lupini, A. R.; Bentley, J.; Pennycook, S. J.; Anderson, I. M.; Minor, A. M.; Schmid, A. K.; Duden, T.; Radmilovic, V.; Ramasse, Q. M.; Watanabe, M.; Erni, R.; Stach, E. A.; Denes, P.; Dahmen, U., *Microsc. Microanal.* **2008,** *14*, (5), 469-477.

(3) Sasaki, T.; Sawada, H.; Hosokawa, F.; Kohno, Y.; Tomita, T.; Kaneyama, T.; Kondo, Y.; Kimoto, K.; Sato, Y.; Suenaga, K., *J. Electron Microsc.* **2010,** *59*, S7-S13.

(4) Li, X. L.; Wang, X. R.; Zhang, L.; Lee, S. W.; Dai, H. J., *Science* **2008,** *319*, (5867), 1229-1232.

(5) Moser, J.; Barreiro, A.; Bachtold, A., *Appl. Phys. Lett.* **2007,** *91*, (16), 163513.

(6) Huang, J. Y.; Qi, L.; Li, J., *Nano Res.* **2010,** *3*, (1), 43-50.

(7) Qi, H.; Qian, C.; Liu, J., *Nano Lett.* **2007,** *7*, (8), 2417-2421.